International Journal of Signal Processing, Image Processing and Pattern Recognition
Vol.7, No.2 (2014), pp.85-98
http://dx.doi.org/10.14257/ijsip.2014.7.2.09

A Novel Approach for Shaken Image Deblurring

Quang Thi Nguyen[1], Yong Gang Cao[1,2], Guang Wen Liu[1],
Nghia Pham Minh[3] and Van Nhu Le[3]

[1]*Changchun University of Science and Technology – China*
[2]*Changchun Institute of Optics, Fine Mechanics and Physics - Chinese Academy of Sciences - China,*
[3]*Harbin Institute of Technology, China*
thinqmta@gmail.com

Abstract

Blurry images are the bane of many photographers. Although sometimes these images could be retaken in the hope that the next exposure will not be blurred, but frequently they are of some unique event that could only be captured once. The most common cause of blurry images is camera shake. Camera shake means that during the exposure the camera moved. This movement may be very small but still creates blurry images. In this paper, a novel blind-deblurring approach for removing the effect of camera shake from blurry image is proposed. Starting with an image that has been blurred by camera shake, we recover the unknown shape image in two phases: (i) a kernel estimation phase using Radon transform method, and (ii) the shape image recovery based on EM algorithm. Comprehensive comparisons on a number of blurry images show that our approach is not only substantially faster, but it also leads to better deblurring results. Our experimental results are also shown for comparisons. Visually, we find that the restored images are better than those given by the algorithm in other methods from previous works.

Keywords: *Camera shake, blind deconvolution, blur kernel, radon transform, kernel estimation*

1. Introduction

Camera shake is a common effect in many images, since the resulting blur spoils many photos taken in low-light conditions. The shake effect can be reduced by using faster exposures, but we cannot avoid other effects such as sensor noise or ringing effect. Much significant progress has been made recently towards removing this blur from images. The model of camera shake that describes the camera motion during exposure is the blur kernel in convolution operation. Restoring the sharp latent image from its blurred image without knowing the camera motion that took place during the exposure is thus a form of blind image deconvolution. Camera shake can be classified into two categories: (i) PSF variation across the image, *i.e.*, how point sources would be recorded at different locations on the sensor, and (ii) Camera's motion varies the image and how the depth of the scene varies.

We assume the scene to be static in our approach, *i.e.*, only the camera moves, and none of the photographed objects (no object motion). In this paper, we consider the problem of "blind" deblurring, where only a single blurry image is available with assuming that blur is uniform blur and camera rotation is negligible. We apply our model within using the Radon transform for kernel estimation case and S. Cho *et al.* [8] for the case of non-blind deblurring.

ISSN: 2005-4254 IJSIP

2. Related Work

Most of the recent work has investigated the automatic estimation of kernel for the blur caused by camera shake. Joshi *et al*. [18] use inertial measurement sensors to estimate the motion of the camera over the course of the exposure, the experiment results show a clear improvement over the input blurry image but there is still some residually ringing that is unavoidable due to frequency loss during blurring. Michael Hirsch *et al*. [30] proposed a forward model based on the efficient filter flow framework, incorporating the particularities of camera shake. That approach does not deal with moving or deformable object, or scenes with significant depth variation. Stefan Harmeling *et al*. [31] introduced taxonomy of camera shake and constructed a method for blind deconvolution in the case of space-variant blur based on a recently introduced framework for space-variant filtering. The disadvantage of method is that it can fail if the blurs are too large or if they vary too quickly across the image. Sophisticated algorithms for non-blind deconvolution have recently been proposed (Dabov *et al*. [11]; Shan *et al*. [26]; Yuan *et al*. [29]), but their application has generally been limited to the case of uniform blur. Note however that Tai *et al*. [27] propose a modified version of the Richardson-Lucy algorithm for deblurring scenes under general projective-motion, where the temporal sequence of projective transformations which caused the blur is known. Fergus *et al*. [12] used a zero-mean Mixture of Gaussian to fit the heavy-tailed natural image prior. Levin *et al*. [21] showed that common MAP methods involving estimating both the image and kernel will likely fail because they favor the trivial solution. Joshi *et al*. [17] predicted sharp edges by first locating step edges and then propagating the local intensity extrema towards that edge. When the blur kernel is known, the process of restoring a blurred image is referred to as non-blind deconvolution. Richardson-Lucy (RL) or Weiner filtering is known to be sensitive to noise. Yuan *et al*. [29] proposed a progressive multi-scale refinement scheme based on an edge preserving bilateral Richardson-Lucy (BRL) method. Joshi *et al*. [19] incorporated a local two-color prior to suppress noise.

Actually, most of proposed deconvolution methods still have disadvantages in output image, for example the ringing effect. In our proposed method, we use EM algorithm to avoid these undesirable effects.

3. Blur Model and Proposed Algorithm

3.1. Image and Blur Model

The blur model can represent a blurred image b as a convolution of the latent image l with a blur kernel k plus additional image noise n:

$$b = k \otimes l + n \tag{1}$$

where $\otimes$ is the convolution operator, n denotes sensor noise at each pixel. The problem of blind-deconvolution is to recover the latent image l from blurred image b without specific knowledge of blur kernel k.

Blind deconvolution is typically addressed by first estimating the kernel, and then estimating the sharp image when the kernel is known. This method is not an exception. The deblurring implementation is classified into two main steps. In the first step, the blur kernel is estimated by using the Radon transform. Then we apply non-blind deconvolution with the outlier handling algorithm [8] for estimating the latent image in the second step. Therefore, our algorithm is implemented in following steps:

Step 1: Detect step edge in the blurry image so as to construct the Radon projection

Step 2: Construct the Radon projection of blur kernel using estimated color step edge in step 1.

Step 3: Recover the blur kernel from its projections

Step 4: Reconstruct the latent image using the estimated blur kernel in step 3

3.2. Blur Kernel Estimation

3.2.1. The Radon Transform

Applying the Radon transform on an image $f(x, y)$ for a given set of angles can be thought of as computing the projection of the image along the given angles. The resulting projection is the sum of the intensities of the pixels in each direction, *i.e.*, a line integral. The result is a new image $R(f, \rho, \theta,)$. This can be written mathematically by defining

$$\rho = x\cos\theta + y\sin\theta \tag{2}$$

after which the Radon transform can be written as

$$R(f, \rho, \theta) = \int_{-\infty}^{\infty}\int_{-\infty}^{\infty} f(x, y)\,\delta(\rho - x\cos\theta - y\sin\theta)\,dxdy \tag{3}$$

where δ (□) is the Dirac delta function.

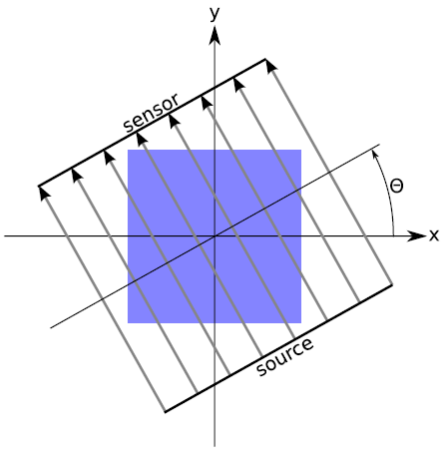

Figure 1. Model of Radon Transform with Orientations θ

The Radon transform is a mapping from the Cartesian rectangular coordinates (x, y) to a distance and an angel (ρ, θ), also known as polar coordinates. The function $R(f, \rho, \theta,)$ can be viewed as projection of $f(x, y)$ along the direction orthogonal to orientation θ (in this case, θ is fixed). With enough projections of f along different orientations θ, the original signal f can be recovered. This is known as the *inverse Radon transform* and is computationally inexpensive. For instance, the commonly used *filtered back-projection* method consists of a "ramp filter" (1-D convolutions) applied

to each projection, followed by back-projection. One way to implement this method is to use 1-D Fourier transforms to convert the 1-D convolutions into products and then use a 2-D inverse Fourier transform.

3.2.2. Edges Detection in Blurry Image

For an accurate kernel reconstruction, we need to find stable, isolated step edges. We introduce an image analysis technique that selects stable edges from a blurry image. As a first step, we run an edge detector to find an edge map *E* of candidate edge samples.

Our goal is to sieve isolated step edges that satisfy four desired characteristics. First, selected pixels should correspond to a step edge with enough contrast on either side, which ensures that the signal to noise ratio of the blurred profile is high. We enforce this constraint by discarding edge samples with a small color difference between two locally dominant colors. We measure the edge color c_1 , c_2 and discard the edge sample if $|c_1 - c_2| < 0.03$ in RGB space. Second, the blurred edge profile should not be contaminated by adjacent edges. To ensure that two adjacent step edges are sufficiently separated, we take an orthogonal slice S_E of the edge map *E* at each edge candidate, and we discard edge samples with $\sum S_E > 1$. Third, a local neighborhood of an edge candidate should conform to a color-line image model. In other words, blurred edge profiles should lie between 0 and 1. An edge sample with a slice that lies outside of $0 - \varepsilon$ and $1 + \varepsilon$, where $\varepsilon = 0.03$, is discarded. Lastly, the edge should be locally straight. The "straightness" is measured as the norm of the average orientation phasor in the complex domain. At each edge candidate *m*, we compute the following measure:

$$\frac{\left\| \sum_{j \in \square(m)} \exp\left(-i2\theta_j\right) \right\|}{\sum_{j \in \square(m)} 1} \tag{4}$$

where $i^2 = 1$, and $\square(m)$ indicates edge candidates in the neighborhood of pixel *m*. If this norm is close to 1, then the edge is locally straight in the neighborhood of pixel *m*. We discard edge samples with the norm less than 0.97.

Our edge selection algorithm depends on the blur kernel size, which is estimated by users. If the estimated blur kernel size is too large, the second and third step of our edge selection algorithm would reject many edges since (i) more slices of the edge map *E* would contain more than one edge (ii) the size of the neighborhood in which the color-line model should hold increases. Therefore, users should ensure that the estimated blur size is just enough to contain the blur.

3.2.3. Recovering the Blur Kernel

For recovering the blur kernel from its projections, we first compute a Radon projection from a color step edge. We can formulate the convolution of the kernel with the image of an ideal line as a line integral of the kernel. Without loss of generality, our method will be implemented with assuming $\theta = 0$, the situations for other orientation can be derived simply by rotating the axes.

We begin our approach by considering a binary step edge

$$H(x,y) = \begin{cases} 1 & if\ x \geq 0 \\ 0 & otherwise \end{cases} \tag{5}$$

Defining an ideal color step edge as $E = Hc_1 + (1-H)c_2$ we can obtain the convolution of the kernel with this edge:

$$B_E = c_1(k \otimes H) + c_2(1 - k \otimes H) \tag{6}$$

where $B_E = k \otimes E$ is blurred version of E, c_1 and c_2 have measured from (§3.2.2).

We seek to retrieve $B_H = k \otimes H$ that describes the blurred edge independent of its colors: at each pixel, we have three equations, one for each RGB channel, of the form $B_E = B_H c_1 + (1 - B_H)c_2$. Since B_H is the only unknown, this is an over-constrained linear system that can be solved with a least-squares formulation, which in practice is a simple average of the solutions from each RGB channel.

After obtaining scalar description of the blurred edge $B_H = k \otimes H$, we seek to derive the blurred line response from the blurred edge response.

From definition of $H(x,y)$ in (5) we have:

$$H(x,y) = \int_{-\infty}^{x} \delta(t)\,dt$$

$$\Rightarrow \quad \frac{\partial H}{\partial x}(x,y) = \delta(x) \tag{7}$$

Taking the derivative of B_H in the *x* direction, we obtain:

$$B_L = \frac{\partial B_H}{\partial x} = k \otimes \frac{\partial H}{\partial x}(x,y) \tag{8}$$

Combining (7) and (8) we obtain:

$$B_L = \frac{\partial B_H}{\partial x} = k \otimes \delta_x \tag{9}$$

where $\delta_x(x,y) = \delta(x)$.

We show that sampling B_L horizontally produces a vertical Radon projection of the kernel, from (9), we get $B_L(x,y)$ by expanding $k \otimes \delta_x$ (we can omit y in this case because the formula does not depend on it)

$$B_L(x) = \iint k(u,v)\delta(x-u)\,du\,dv \tag{10}$$

Considering equation (2) in the case $\theta = 0$, we realize that $B_L(x)$ is the Radon transform in vertical $R(k,x,0,)$ of blur kernel k.

To reconstruct an accurate blur kernel, the projections must be consistently aligned with each other. For this, we exploit the fact that the center of mass of the kernel projects onto the center of mass of each projection. In practice, we compute a first estimate of each projection and then shift it to align its center of mass on the origin of the coordinate system.

We seek to recover the blur kernel from its projections $\tilde{R}_i$ along the direction θ_i by adding a priori knowledge about blur kernels. Using Bayesian formulation, we seek to maximize the posterior probability $p(k \mid b)$ of the blur kernel k given the observed image b. We use a classical decomposition into a likelihood term and a prior: $p(k \mid b) \propto p(b \mid k)\, p(k)$. To model the likelihood term $p(b \mid k)$, we define the linear operator $\int_\theta$ that computes a line integral in the direction θ and seek to satisfy the constraint that the actual projections $\int_{\theta_i} k$ of the blur kernel should match our measured projections $\tilde{R}_i$:

$$p(b \mid k) \propto \exp\left(\frac{1}{2\eta_{obs}^2} \sum_{i=1}^{N} \left\| \tilde{R}_i - \int_{\theta_i} k \right\|^2 \right) \tag{11}$$

where N is number of Radon projections $\tilde{R}_i$ that were extracted from image, η_{obs}^2 is the variance of observation noise that comes from the inaccuracies in the estimation of the orientation θ. Because of estimating the projections $\tilde{R}_i$ with finite differences for first derivative, the impact of noise is doubled. A factor (α) were added to the orientation noise. This gives $\eta_{obs}^2 = (2 + \alpha)\eta_{img}^2$. Use cross-validation for setting α to 1.

The kernel prior with knowledge the intensity profiles of blur kernel are sparse:

$$p(k) \propto \exp\left(-\lambda_1 \|k\|^{\gamma_1} - \lambda_2 \|k\|^{\gamma_2} \right) \tag{12}$$

In practice, we minimize the negative log-posterior $-\log\left(p(b \mid k)\, p(k)\right)$ with an iterative re-weighted least–square method. $\lambda_1 = 1.5$, $\lambda_2 = 0.1$, $\gamma_1 = 0.9$ and $\gamma_2 = 0.5$ were used in whole experiment.

In practice, for speeding up the computation, we average out the noise and then behaving the optimization by binning projection with similar orientations.

We define a small set of n orientations $\hat{\theta}_j$ with $n \ll N$ and group the measured values $\hat{\theta}_j$ according to their nearest $\hat{\theta}_j$. This forms sets P_j of i indexes. For each non-empty set, we compute the average projection $\hat{R}_j = \frac{1}{\omega_j} \sum_{i \in P_j} \tilde{R}_i$ where ω_j is the size of P_j. We then reformulate the likelihood as:

$$\exp\left(-\frac{1}{2\eta_{obs}^2} \sum_{j=1}^{n} \omega_j \left\| \hat{R}_j - \int_{\theta_j} k \right\|^2 \right) \tag{13}$$

3.3. Image Reconstruction

After having estimated and fixed the kernel, we recover the final shape image by using non-blind deconvolution method proposed by S. Cho *et al.*, [8]. Previous non-blind deconvolution methods assume a linear blur model where the blurred image is generated by a linear convolution of the latent image and the blur kernel. This assumption often does not hold in practice due to various types of outliers in the imaging process. Without proper outlier

handling, recent methods may generate results with severe ringing artifacts even when the kernel is estimated accurately.

In previous work, S. Cho *et al*., [8] demonstrate that outliers violate the linear blur assumption and consequently cause severe ringing artifacts to the result image. It is inappropriate to use a linear blur model when outliers exist, so it is necessary to avoid the violation of outliers, but most sources of the outliers are inevitable unfortunately. The method that masks out the outliers, Harmeling *et al*. [14], involves a threshold which distinguishes the outliers for masking out, but there is no guidance on how to find the optimal threshold value, so that method is not robust enough. Yuan *et al*. [29] proposed a directly suppressing artifacts approach, that method actually handle the outliers implicitly. We propose an EM method which handle the outliers directly, and that is more efficient.

In this paper, we use the MAP model for computing the most probable latent image *l*:

$$L = \arg\max p(l \mid k, b) \tag{14}$$

According to the Bayes's theorem:

$$L = \arg\max_{l} \sum_{r \in R} p(b \mid r, k, l)\, p(r \mid k, l)\, p(l) \tag{15}$$

where *R* is the space of all possible configurations of *r*.

We then define the latent image prior *p(l)* as:

$$p(l) = \exp(-\lambda \varphi(l)) / Z \tag{16}$$

where *Z* is a normalization constant. Using the sparse prior, we set $\phi(l) = \sum_{i} \{ | (\nabla^{h} l)_i |^{\alpha} + | (\nabla^{v} l)_i |^{\alpha} \}$. We use $\alpha = 0.8$ in our experiments

Use EM method for solving (15), we have:

$$L_{E-\log} = E[\log p(b \mid r, k, l) + \log p(r \mid k, l)] \tag{17}$$

Since we assumed that noise is spatially independent, the likelihood $p(b \mid r, k, l) = \prod_{i} p(b_i \mid r, k, l)$, then, based on our noise model, we define:

$$p(b_i \mid r, k, l) = \begin{cases} \hat{N}(b_i \mid f_i, \sigma) & if \quad r_i = 1 \\ C & if \quad r_i = 0 \end{cases} \tag{18}$$

where $f = k \otimes l$, $\hat{N}$ is a Gaussian distribution, σ is the standard deviation. *C* is a constant defined as the inverse of the width of the dynamic range in the input image.

According to the prior model, with assuming *r* is spatially independent, $p(r \mid k, l) = \prod_{i} p(r_i \mid f_i)$, we then define:

$$p(r_i = 1 \mid f_i) = \begin{cases} P & if \quad f_i \in R \\ 0 & if \quad f_i \notin R \end{cases} \tag{19}$$

where R is dynamic range, $P \in [0,1]$ is the probability that pixel i is inlier . We set $R = [0,1]$ for our implementation.

After putting (18), (19) into (17), we have:

$$L_{E-\log} = -\sum_i \frac{E[r_i]}{2\sigma^2} | b_i - f_i |^2 \tag{20}$$

where $E[r_i] = p(r_i = 1 | b, k, l^0)$, by the Bayes' theorem, combination of (18) and (19) can be obtained:

$$E[r_i] = \begin{cases} \dfrac{\hat{\mathrm{N}}(b_i | f_i^0, \sigma) P}{\hat{\mathrm{N}}(b_i | f_i^0, \sigma) P + \mathrm{C}(1-P)} & if \quad f_i^0 \in R \\ 0 & if \quad f_i^0 \notin R \end{cases} \tag{21}$$

where $E[r_i]$ is approximate 1 if the observed pixel i is inlier, and otherwise $E[r_i] = 0$

Use M step for finding the revised estimate L such that:

$$L_{output} = \arg\max_l \left\{ L_{E-\log} + \log p(l) \right\} \tag{22}$$

The values which computed in E step ($E[r_i]$) are used as pixel weights in the deconvolution process. That process is performed in the M step. As a result, only inliers with large weights are used for deconvolution in the M step, while outliers with low weights are excluded.

We use the iteratively re-weighted least squares (IRLS) method for solving (23), which is equivalent to minimizing:

$$L = \sum_i \omega_i^r | b_i - (k * l)_i |^2 + \lambda \left\{ \sum_i \{ \omega_i^h | (\nabla^h l |_i)^2 + \omega_i^v | (\nabla^v l |_i)^2 \} \right\} \tag{23}$$

where $\omega_i^r = E[r_i] / 2\sigma^2$, $\omega_i^h = | (\nabla^h l)_i |^{\alpha-2}$, $\omega_i^v = | (\nabla^v l)_i |^{\alpha-2}$, we finally get the latent gradient image by alternating between updating (ω_i^h ; ω_i^v) and minimizing (23).

3.4. Kernel Size Optimization

In proposed method for kernel estimation and deconvolution, we can obtain the kernel and deblurred image from input blur image but we don't know which size of kernel is better, and when output deblurred image will reach the desired quality. This is also an ill-posed problem in recent research about blind deconvolution. The quality of output image depends on size of kernel. The optimal size of kernel (corresponding to the best quality of image) is different in each blur image.

The proposed method performed estimation by varying image resolution in a coarse-to-fine manner. At the coarsest level, k is 3 x 3 kernel. To ensure a correct start to the algorithm, we manually specify the initial 3 x 3 blur kernel to one of two simple patterns. The initial estimate for the latent gradient image is then produced by running the inference scheme,

while holding *k* fixed. We then work back up the pyramid running the inference at each level. At the finest scale, the inference converges to the full resolution kernel *k*.

Table 1. The Value of Average Difference with Different Size of Kernels

PSF Size	Bird.jpg	Fishes.jpg	Lion.jpg	Building.jpg
11*11	0.0200	0.0293	0.0668	0.4275
13*13	0.0214	0.0394	0.0786	0.3364
15*15	0.0126	0.0501	***0.0128***	***0.1929***
17*17	0.0185	0.0532	0.5243	0.4275
19*19	***0.0043***	0.0552	4.2777	0.3108
21*21	0.0047	0.0247	2.7862	0.4861
23*23	0.0036	0.0263	0.3460	0.7682
25*25	0.0157	***0.0080***	0.6935	1.0469
27*27	0.2444	0.0162	1.0194	1.2087
29*29	0.2894	0.1040	1.2385	1.5126
31*31	0.3148	0.1040	2.3672	1.8504

Figure 2. Experimental Results with Different Size of Kernels, Best Results are Obtained in (c), (g), (j) and (n)

We also use Average Difference parameter (AD) for estimating output image:

$$AD = \left| \sum_{j=1}^{M} \sum_{k=1}^{N} \left(x_{j,k} - x'_{j,k} \right) / MN \right| \tag{24}$$

where M x N is size of blur image and deblurred image, after deconvolution process.

This parameter is used because it is simple to calculate, have a clear physical meaning, and is mathematically convenient in the context of optimization. In practice we

found the output deblurred image can reach highest quality with minimum value of Average Difference, and the ringing artifacts in deblurred image are serious at large value of AD, as illustrated in Table 1 and Figure 2.

The results of deconvolution with different kernels are present in Figure 2. Figures. 2(c), (g) (i), (n) are output deconvolution with (19x19) kernel in "Bird.jpg", (25x25) kernel in "Fishes.jpg", (11x11) kernel in "Lion.jpg" and (15x15) kernel in "Palace.jpg" respectively. Clearly these images are deblurred better than others that are deblurred with another size of kernel, the ringing artifacts are suppressed in these cases.

4. Experimental Results and Comparisons

We have demonstrated proposed algorithm and R. Fergus *et al*'s algorithm [12] with the same size of blur kernel in MATLAB and have given some other results for comparisons.

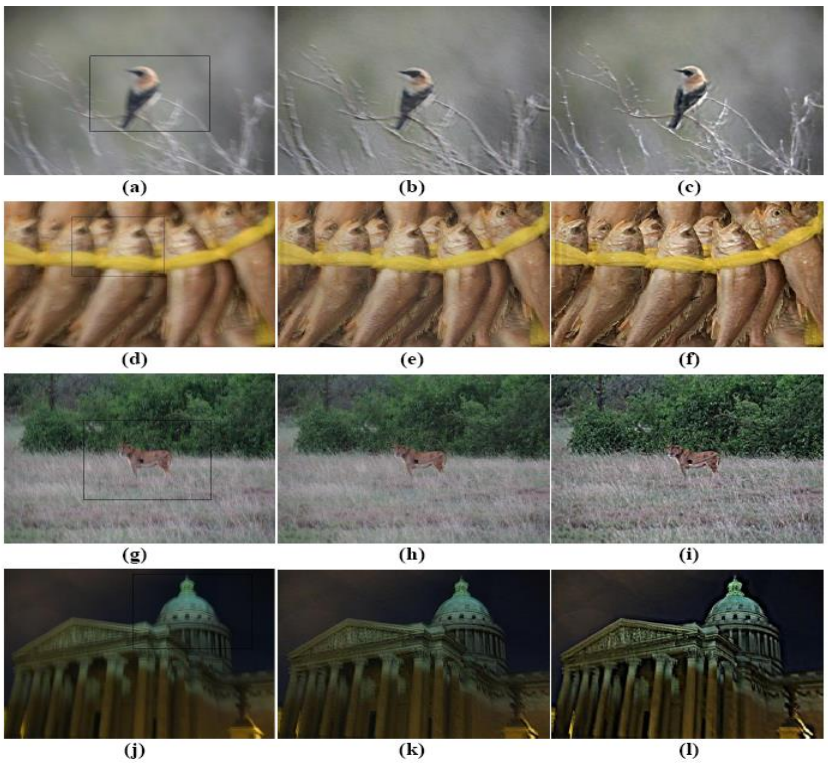

Figure 3. Comparisons to the Method of Fergus *et al*

The input observed images are shown in Figures. 3(a), (d), (g), (j) and (m) (first column). We display the restored images by algorithm in [12] in Figures. 3(b), (e), (h), (k) and (n) (second column), and the images restored by our algorithm are shown in Figures. 3(c), (f) (i), (l) and (o) (third column) respectively. According to the restoration results, the proposed algorithm can recover the image quite well. Visually, we find that the restored images (third column) are clearer, brighter than those given in R. Fergus *et al's*., algorithm [12].

The shadow around the bird is reduced in Figure 3(b) (R. Fergus *et al's*., Algorithm) and those effects have almost disappeared in Figure 3(c) (our algorithm). The tree branches in Figure. 3(c) are also clearer than those branches in Figures. 3(a) and (b).

The shaken effect is also removed completely in Figures 3(f), (i), (l) and (o) (third column). In addition, edges of objects are shown clearly in our results.

We show the closed-up parts of the restored images in Figure 4. We display the closed-up parts of restore images by method in [12] and our method, in Figures 3(a), (c), (e), (g), Figures 4(b), (d), (f), (h) respectively. Again it is clear that the proposed algorithm can restore images quite well.

We have tested the effects of the proposed algorithms for shaken blurs. We can realize the performance of the proposed algorithm is better than other methods.

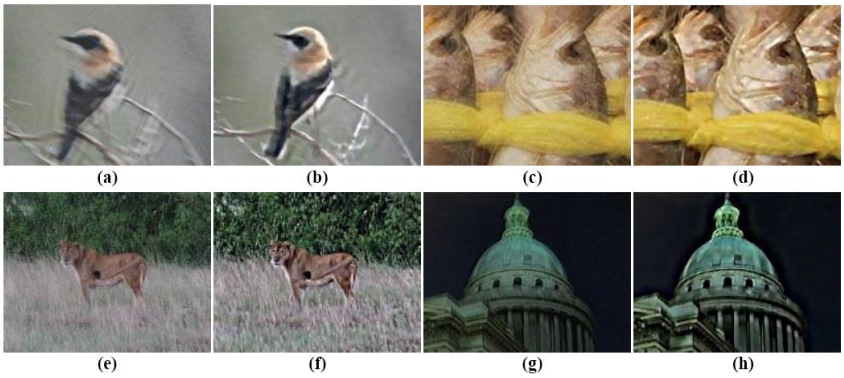

Figure 4. Closed-up Patches of the Restored Images and Comparisons to the Method of Fergus *et al*

5. Conclusion

In this paper, an accuracy improvement method for removing shaken effects from photographs has been proposed. By using proposed method, we can not only increase the robustness of kernel estimation but also obtain an accuracy quality of latent image. However, our method does not behave as well when there are not enough edges in different orientations or when we do not detect enough edges, this problem cause that we can not retrieve Radon projections with enough precision with a sufficient diversity of orientations. Such an approach may prove useful in other computational photography problems. The results of our method still contain artifacts; most prominently, ringing artifacts occur near saturated regions and regions of significant object motion. We suspect that these artifacts can be blamed primarily on the non-blind deconvolution step. We believe that there is significant room for improvement by applying modern statistical methods to the non-blind deconvolution problem in future works.

References

[1] N. Apostoloff and A. Fitzgibbon, "Bayesian video matting using learnt image priors", Conf. on Computer Vision and Pattern Recognition, **(2005)**, pp. 407-414.
[2] M. R. Banham and A. K. Katsaggelos, "Digital image restoration", IEEE Signal Processing Magazine, vol. 14, no. 2, **(2007)**, pp. 24–41.
[3] C. M. Bishop, "Pattern Recognition and Machine Learning", Springer, **(2006)**.
[4] L. Bar, N. Sochen and N. Kiryati, "Image deblurring in the presence of impulsive noise", International Journal of Computer Vision, 70(3), pp. 279–298 **(2006)**
[5] J. F. Cai, H. Ji, C. Liu and Z. Shen, "Blind motion deblurring from a single image using sparse approximation", Proc. CVPR, **(2009)**.
[6] P. Campisi and K. Egiazarian, "Blind image deconvolution: theory and applications", CRC Press, **(2007)**.

[7] J. Caron, N. Namazi and C. Rollins, "Noniterative blind data restoration by use of an extracted filter function", Applied Optics, vol. 41, no. 32, **(2002)** November, pp. 68-84.
[8] J. Chen, L. Yuan, C. K. Tang and L. Quan, "Robust dual motion deblurring", **(2008)**, Proc. CVPR.
[9] S. Cho, J. Wang and S. Lee, "Handling Outliers in Non-Blind Image Deconvolution", IEEE Conf., **(2011)**, pp. 495-502.
[10] S. Cho, Y. Matsushita and S. Lee, "Removing non-uniform motion blur from images", Proc. ICCV 2007, **(2007)**, pp. 1-8.
[11] S. Cho and S. Lee, "Fast motion deblurring", ACM Trans. Graphics (Proc. SIGGRAPH Asia 2009), vol. 28, no. 5, **(2009)**, pp. 145:1–145:8.
[12] K. Dabov, A. Foi, V. Katkovnik and K. Egiazarian, "Image restoration by sparse 3D transform-domain collaborative filtering", SPIE Electronic Imaging, **(2008)**.
[13] R. Fergus, B. Singh, A. Hertzbann, S. T. Roweis and W. Freeman, "Removing camera shake from a single photograph", ACM T. Graphic, vol. 25, **(2006)**, pp. 787-794.
[14] A. Gupta, N. Joshi, C. L. Zitnick, M. Cohen and B. Curless, "Single image deblurring using motion density functions", Proc. ECCV, **(2010)**.
[15] S. Harmeling, S. Sra, M. Hirsch and B. Scholkopf, "Multiframe blind deconvolution, super-resolution, and saturation correction via incremental EM", Proc. ICIP 2010, **(2010)**, pp. 3313-3316.
[16] J. Jia, "Single Image Motion Deblurring Using Transparency", CVPR, **(2007)**.
[17] M. Jordan, Z. Ghahramani, T. Jaakkola and L. Saul, "An introduction to variational methods for graphical models", Machine Learning, vol. 37, **(1999)**, pp. 183-233.
[18] N. Joshi, "Enhancing photographs using content-specific image priors", PhD thesis, University of California, San Diego, **(2008)**.
[19] N. Joshi, S. B. Kang, C. L. Zitnick and R. Szeliski, "Image deblurring using inertial measurement sensors", ACM Trans. Graphics (Proc. SIGGRAPH 2010), vol. 29, no. 4, **(2010)**, pp. 30:1-30:9.
[20] N. Joshi, C. L. Zitnick, R. Szeliski and D. J Kriegman, "Image deblurring and denoising using color priors", CVPR, **(2009)**, pp. 1550-1557.
[21] T. S. Cho, S Paris, B. K. P. Horn and W. T. Freeman, "Blur Kernel Estimation using Radon Transform", CVPR, **(2011)**.
[22] A. Levin, Y. Weiss, F. Durand and W. T. Freeman, "Understanding and evaluating blind deconvolution algorithms", CVPR, **(2009)**.
[23] S. H. Lim and A. Silverstein, "Estimation and removal of motion blur by capturing two images with different exposures", Technical Report HPL-2008-170, HP Laboratories, **(2008)**.
[24] L. B. Lucy, "An iterative technique for the rectification of observed distributions", Astronomical Journal, vol. 79, no. 6, **(1974)**, pp. 745-754.
[25] J. Miskin and D. J. C. Mackay, "Ensemble Learning for Blind Image Separation and Deconvolution", Adv. in Independent Component Analysis, M. Girolani, Ed. Springer-Verlag, **(2000)**.
[26] L. I. Rudin, S. Osher and E. Fatemi, "Nonlinear total variation based noise removal algorithms", Physica. D, vol. 60, **(1992)**, pp. 259-268.
[27] Q. Shan, J. Jia and A. Agarwala, "High-quality motion deblurring from a single image", SIG-GRAPH, **(2008)**.
[28] Y. W. Tai, P. Tan, L. Gao and M. S. Brown, "Richardson-Lucy deblurring for scenes under projective motion path", Technical report, KAIST, **(2009)**.
[29] F. Tsumuraya, N. Miura and N. Baba, "Iterative blind deconvolution method using Lucy's algorithm", Astron. Astrophys, vol. 282, **(1994)** February 2, pp. 699-708.
[30] L. Yuan, J. Sun, L. Quan and H. Y. Shum, "Progressive inter-scale and intra-scale non-blind image deconvolution", ACM Trans. Graphics, **(2008)**.
[31] M. Hirsch, J. Christian, Schuler, S. Harmeling and B. Scholkopf, "Fast Removal of Non-uniform Camera Shake", Proc. IEEE International Conference on Computer Vision, **(2011)**.
[32] S. Harmeling, M. Hirsch and B. Scholkopf, "Space-Variant Single-Image Blind Deconvolution for Removing Camera Shake", NIPS Conference, **(2010)**.
[33] G. S. Watson, "Statistics on spheres", John Wiley and Sons, **(1983)**.

Authors

Quang Thi Nguyen, male, was born in 1980. He received the B.S., M.S. degrees from the Le Quy Don Technical University, Hanoi, Vietnam, in 2004 and 2008, respectively. Now he is pursuing Ph.D. degree in School of Electronics and Information Engineering,

Changchun University of Science and Technology. He currently focuses on blind deconvolution, image processing and pattern recognition.

Yong Gang Cao, male, was born in 1972. He received the B.S. degree from Changchun Institute of Optics and Fine Mechanics in 1996. He is working in Changchun Institute of Optics, Fine Mechanics and Physics, Chinese Academy of Sciences. He is now pursuing Ph.D degree in Changchun University of Science and Technology. His research interests are image processing and pattern recognition.

Guang Wen Liu, male, was born in 1971. He received the B.S., M.S. degrees from the Changchun University of Science and Technology, in 1996 and 2003, respectively, and the Ph.D Degree in Changchun University of Science and Technology, in 2009. He is currently a Associate Professor of School of Electronics and Information Engineering, Changchun University of Science and Technology. His research interests are electronic imaging, digital signal processing and pattern recognition.

Nghia Pham Minh, male, was born in 1980. He received the B.S., M.S. degrees from the Le Quy Don Technical University, Hanoi, Vietnam, in 2005 and 2008, respectively. Now he is pursuing Ph.D. degree in School of Electronics and Information Technology at Harbin Institute of Technology (HIT), Harbin, China. He currently focuses on digital signal processing, Image Processing.

Nhu Le Van, male, was born in 1982. He received the B.S degrees from the Le Quy Don Technical University, Hanoi, Vietnam, in 2007 and M.S dgree from Harbin Institute of Technology in 2012. Now he is pursuing Ph.D. degree in Research center for Space Optics Engineering, Harbin Institute of Technology, Harbin, China. He currently focuses image processing, optic image processing and design optic system.